Volume 2
Number 5
7 March 2021
Pages 1415–1776

Materials Advances

rsc.li/materials-advances

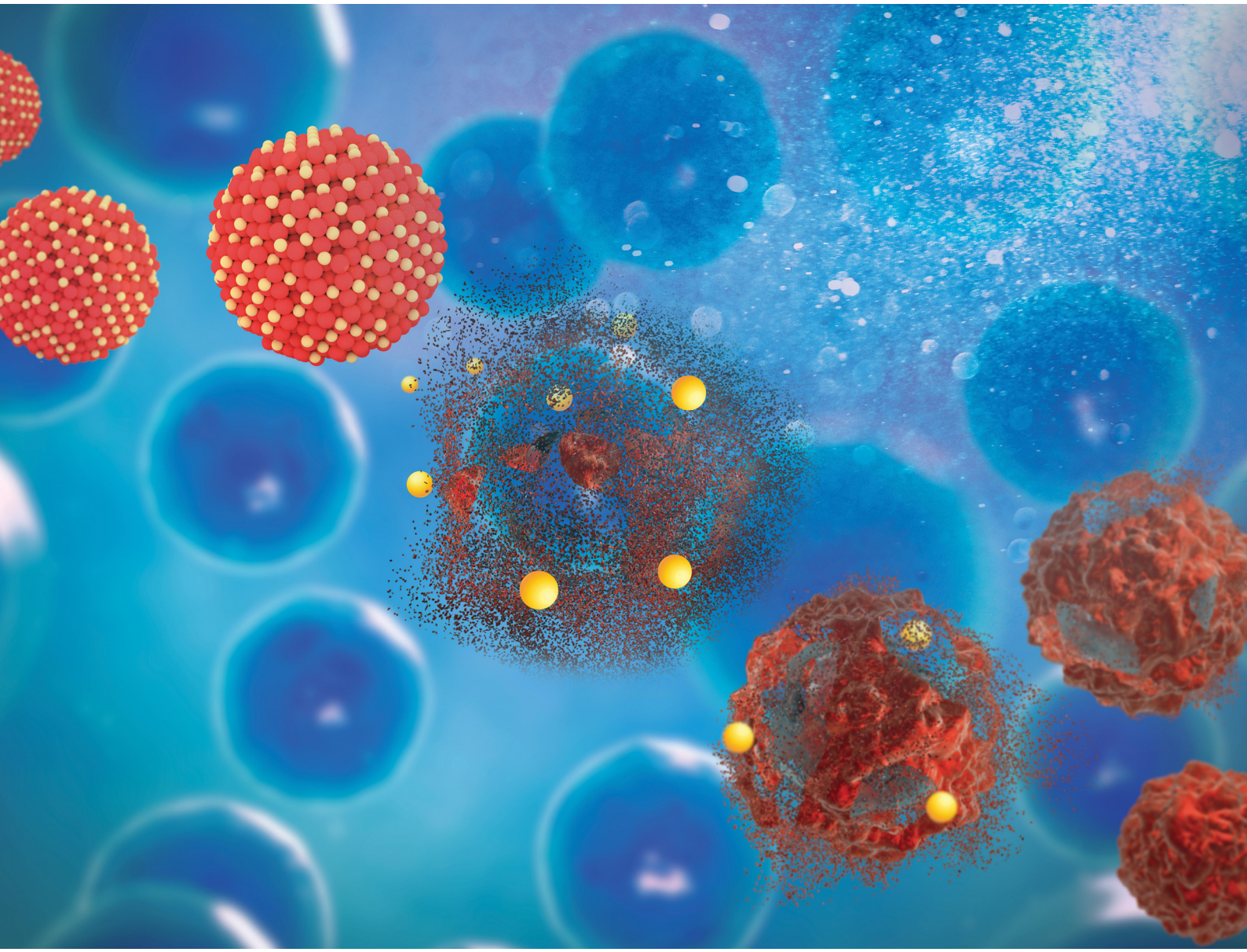

ISSN 2633-5409

ROYAL SOCIETY OF CHEMISTRY

PAPER

Rosa Fernandes, Tito Trindade, Tomás Torres, João P. C. Tomé *et al.*
Encapsulation of glycosylated porphyrins in silica nanoparticles to enhance the efficacy of cancer photodynamic therapy

Materials Advances

ROYAL SOCIETY OF CHEMISTRY

PAPER

View Article Online
View Journal | View Issue

Cite this: *Mater. Adv.*, 2021, **2**, 1613

Encapsulation of glycosylated porphyrins in silica nanoparticles to enhance the efficacy of cancer photodynamic therapy†

Wioleta Borzęcka,[abc] Patrícia M. R. Pereira,[ad] Rosa Fernandes, *[de] Tito Trindade, *[b] Tomás Torres *[cfg] and João P. C. Tomé *[ah]

Received 24th October 2020,
Accepted 12th December 2020

DOI: 10.1039/d0ma00830c

rsc.li/materials-advances

In this study, we encapsulated *S*-galactosylated and *S*-glucosylated porphyrins (Pors) into amorphous silica nanoparticles (SNPs) to enhance the photodynamic therapy (PDT) activity. The resulting galacto- and gluco-nanoformulations were demonstrated to be spherical in shape with diameters of 197.3 ± 29.0 nm and 128.3 ± 22.2 nm. The galacto- and gluco-nanoparticles (NPs) were able to produce a high amount of singlet oxygen ($^1O_2$) and were stable under the conditions of the experiments. *In vitro* studies show that the nanoformulations were effectively taken up by the human bladder cancer cell lines HT-1376 and UM-UC-3. The PDT results show that these photoactive nanoformulations are 3 to 5 times more efficient than the non-encapsulated/free Pors. These Por–silica nanoformulations could be successfully used as novel nanocarriers for the delivery of photosensitizer materials for cancer PDT.

Introduction

PDT is a promising therapeutic procedure used in cancer treatment, which combines three components: a drug, visible or near-infrared light and molecular oxygen. On their own these elements do not have any cytotoxic effects; however, when combined they can produce cytotoxic reactive oxygen species (ROS). Increased levels of ROS can elicit oxidative stress and cancer destruction, *via* direct cancer cell damage and/or activation of an immune response against cancer cells.[1–4] The advantage of using PDT over other cancer treatments (*e.g.* surgery, chemotherapy, and radiotherapy) is that it has lower toxic effects on biological systems.[5] PDT was approved by the Food and Drug Administration (FDA) as a clinical protocol for cancer treatment more than 20 years ago, and since then many photosensitizers (PSs) have been developed for PDT, such as HpD, Photofrin, or Temoporfin.[6] However, nowadays most of the available PSs are based on the tetrapyrrole structure such as porphyrins with larger hydrophobic groups attached and their solubility in aqueous solutions is often poor, restricting them in clinical applications. Moreover, PDT still has limitations for use as a general protocol to treat cancer. Thus, there is still a need to study alternatives to improve the efficiency of PDT and overcome its limitations, such as low effectiveness in treating large tumors or causing burns, swelling, pain, scarring in nearby healthy tissues or persistent skin photosensitization. For that, it is crucial to not only improve efficient irradiation systems to deliver the activating light, but also to develop new powerful and selective PSs. In the context of new PSs, NPs have recently emerged as promising vehicles for PDT agents, overcoming the limitations of PSs such as low water solubility and low targeting properties.[7–11]

Using PSs in different nanoformulations can improve their biocompatibility, blood circulation, and selective accumulation in tumor tissues thanks to the enhanced permeability and retention effect (EPR).[12–14] Among other nanomaterials, silica nanoparticles (SNPs) have emerged as promising vehicles for PDT owing to their biocompatibility, large surface area, controllable size formation, hydrophilic surface and ability of surface functionalization, hence the possibility for tumor targeting through surface modification.[15–19] Moreover, amorphous silica shells

[a] *QOPNA-LAQV-REQUINTE and Department of Chemistry, University of Aveiro, 3810-193 Aveiro, Portugal*
[b] *CICECO-Aveiro Institute of Materials and Department of Chemistry, University of Aveiro, 3810-193 Aveiro, Portugal*
[c] *Department of Organic Chemistry, Autonoma University of Madrid, 28049 Madrid, Spain*
[d] *Coimbra Institute for Clinical and Biomedical Research (iCBR), Faculty of Medicine, University of Coimbra, Azinhaga de Santa Comba, 3000-548 Coimbra, Portugal*
[e] *CNC.IBILI, University of Coimbra, 3000 Coimbra, Portugal*
[f] *IMDEA-Nanociencia, Campus de Cantoblanco, c/Faraday 9, 28049 Madrid, Spain*
[g] *Institute for Advanced Research in Chemical Sciences (IAdChem), Universidad Autónoma de Madrid (UAM), 28049 Madrid, Spain*
[h] *Centro de Química Estrutural & Departamento de Engenharia Química, Instituto Superior Técnico, Universidade de Lisboa, 1049-001 Lisboa, Portugal. E-mail: jtome@tecnico.ulisboa.pt*

† Electronic supplementary information (ESI) available: NPs' preparation and characterization, singlet oxygen studies and dark toxicity studies. See DOI: 10.1039/d0ma00830c

can protect entrapped molecules against chemical and biochemical degradation, but at the same time control their release.[20,21] There are already nanoparticle-based drug delivery platforms which were approved by the FDA and many others under clinical trials.[22–26]

Among other parameters, NPs' interactions with cancer cells depend on the NPs' size, which influences their active and passive cellular internalization, determining the therapeutic targeting.[27] When compared with healthy cells, tumor cells have poor lymphatic drainage and leaky vasculature. Particles with a size ranging from 10 to 500 nm tend to accumulate inside tumor cells and their accumulation is facilitated by lymphatic filtration. On the contrary, very often much smaller ordinary drugs cannot remain in tumors because they return to circulation by a diffusion process.[28,29]

SNPs are platforms that allow covalent and non-covalent immobilization of PSs outside or inside their structures. Recent studies demonstrated that using SNPs combined with Pors could eliminate aggregation of Pors, the hydrophobic nature of PSs or reduced selectivity for targeted tissues and consequently increase the PDT efficiency.[30,31] The pioneering work in this field was described in 2003 by Yan *et al.*,[32] where meta-tetra(hydroxyphenyl)-chlorin embedded into silica nanoparticle platforms demonstrated the ability to generate $^1O_2$. Moreover, the authors have shown that the $^1O_2$ production by the SNPs is higher than the one from the free PS. From that time, scientists have put in a lot of effort to enhance PDT with PS–SNP. For instance, Gao *et al.*[33] in a simple method enhanced the photodynamic selectivity of Pors adsorbed onto SNPs against breast cancer cells. In the same year, He *et al.*[34] developed organically modified silica (ORMOSIL) nanoparticles encapsulated with protoporphyrin IX (PpIX) for direct two-photon PDT. In their research, ORMOSIL nanoparticles were able to successfully destroy HeLa cells. Ho *et al.*[35] also used PpIX with mesoporous silica nanocarriers for selective cancer PDT. These highly efficient, non-cytotoxic drug delivery platforms designed for PDT were phospholipid-capped, PpIX-loaded and fluorescein isothiocyanate (FITC)-sensitized mesoporous silica nanocarriers derivatized with folate. These complex SNPs were effective to kill targeted HeLa human cervical epithelioid carcinoma cells and A549 human lung carcinoma cells *in vitro* and prevent further tumor growth. Miao X. *et al.*[36] were able to overcome the hydrophobic nature of Photosan-II by loading it into hollow SNPs. By this, they eliminated the difficulties with delivery in the physiological environment and the low photophysical properties due to the aggregation of PSs, which decreased the production of $^1O_2$ for PDT. These NPs enhance the photoactivity of the PS against QBC939 cholangiocarcinoma cells. Later, Wen *et al.*[37] proved that these NPs in *in vitro* and *in vivo* experiments on liver cancer in nude mice were more efficient than the PS alone. Qian *et al.*[38] developed Por (HPPH) doped colloidal mesoporous silica nanoparticles for three-photon PDT. The cytotoxic effect of HPPH doped SNP-mediated PDT against HeLa cells was proved.

In the present work 5,10,15,20-tetrakis(4-1′-thio-glucosyl-2,3,5,6-tetrafluorophenyl)porphyrin (SGlc-Por, **PS 1**) and 5,10,15,20-tetrakis(4-1′-thio-galactosyl-2,3,5,6-tetrafluorophenyl)porphyrin (SGal-Por, **PS 2**) were chosen as PS (Scheme 1) platforms because there are a number of reports on the potential of glycosylated porphyrins as PDT agents.[39–43] In our research we used Pors with *S*-glycoside bonds rather than *O*-glycoside because drugs bearing saccharides with *O*-glycoside linkages are readily hydrolyzed by a variety of enzymatic and non-enzymatic acid/base reactions resulting in short half-lives.[44] It is known that aggregation of the PS decreases the efficiency of $^1O_2$ generation. Thus, we decided to deliver PSs inside cancer cells by the use of nanovehicles which could also enhance the stability of these PSs in aqueous media. Hence, PSs were non-covalently encapsulated into an amorphous silica matrix, and then these nanomaterials were studied in cancer PDT.

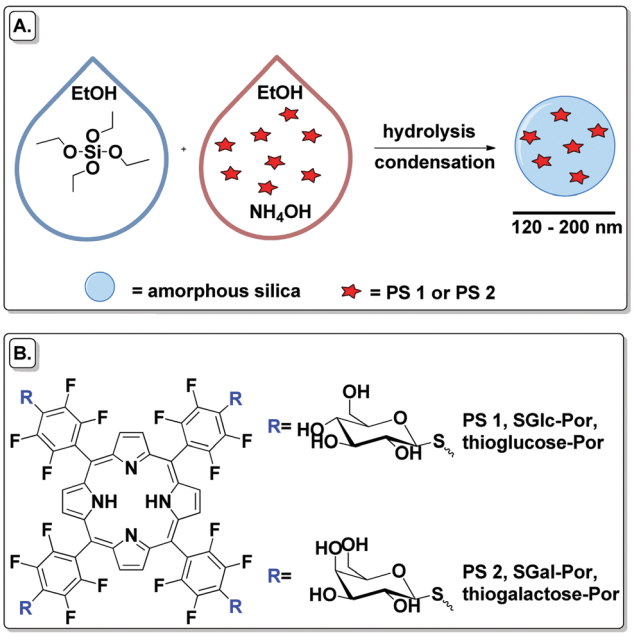

Scheme 1 (A) Schematic preparation of PSs encapsulated into SNPs. (B) Structures of **SGlc-Por** and **SGal-Por** used as free and encapsulated PSs.

Results and discussion

Synthesis of the PSs

S-Glycoside porphyrins **PS 1** and **PS 2** were synthesized according to literature procedures presented elsewhere.[39–43] Briefly, protected carbohydrate porphyrins were obtained by nucleophilic substitution of the *p*-fluorine of the corresponding free-base porphyrin 5,10,15,20-tetrakis(pentafluorophenyl)porphyrin ($TPPF_{20}$) with acetyl 2,3,4,6-tetra-*O*-acetyl-1-thio-D-glucopyranoside or acetyl 2,3,4,6-tetra-*O*-acetyl-1-thio-D-galactopyranoside. Applying a simple synthesis, these Pors bearing four carbohydrate moieties conjugated *via S*-glycoside bonds were obtained in high yields. Final deprotection of the carbohydrate moieties using alkaline hydrolysis afforded the final unprotected *S*-glycoside porphyrins **PS 1** and **PS 2**.

Preparation of SNPs and their PS–SNP hybrids

SNPs and their Por–silica nanoformulations were prepared by the Stöber method in which the hydrolysis and condensation of

tetraethyl orthosilicate (TEOS) is facilitated by a base in ethanol and water (Scheme 1).[45]

To obtain a Por–silica nanoformulation with photodynamic properties it is necessary that the amount of PS inside the NP generates reactive oxygen species and/or that the Por photoproperties do not change much during the nanoformulation steps. The conditions of the NPs' preparation were optimized by varying the amount of base NH_4OH, TEOS and PS (Tables 1–3). Compound **PS 1** was chosen to optimize the reaction conditions. Generally, in a 15 mL falcon tube, each PS was dissolved in EtOH and then NH_4OH was added (the total volume of this mixture was 6.25 mL). The mixture was sonicated for 5 min and TEOS dissolved in EtOH was added (the total volume of this mixture was 1.25 mL). The reaction was incubated for 24 h at 25 °C under continuous agitation (250 rpm) in an incubator shaker (IKA KS 4000 i control) in a horizontal position. After that time, the NPs were isolated by centrifugation (15 mL falcon tubes, 6000 rpm, 30 min) and washed with EtOH. The final NPs were air-dried.

PSs encapsulation optimization studies

Keeping the amount of PS and TEOS constant, three reactions with different amounts of base were performed to determine the amount of encapsulated PS *versus* the amount of base (Table 1). In this case, **PS 1** (2.977 μmol, 0.4 mM) was dissolved in EtOH and then NH_4OH was added. The mixture was sonicated for 5 min and TEOS (0.375 mmol, 50 mM) dissolved in EtOH was added. After 24 h reaction, the NPs were washed and dried at room temperature.

A high concentration of NH_4OH resulted in a small amount of encapsulated **PS 1** in the NPs. A concentration of 0.16 M NH_4OH in the reaction mixture did not allow the formation of nanoformulations (**NP 1**). The concentration of base also influences the size of the NPs. After increasing the concentration of NH_4OH by two times, the size of the NPs increased by almost 5 times (**NP 2** *versus* **NP 3**). The highest concentration of **PS 1** in the final NPs was observed for **NP 2** where a 0.32 M concentration of NH_4OH was used; thus, for further experiments, these conditions were used for the synthesis of the nanoformulations.

Keeping the amounts of PS and base constant, the dependence of the amount of encapsulated PS on the amount of TEOS was determined. For this, **PS 1** (2.977 μmol, 0.4 mM) was dissolved in EtOH and then NH_4OH (2.4 mmol, 0.32 M) was added. The mixture was sonicated for 5 min and TEOS dissolved in EtOH was added (Table 2). After 24 h reaction, the NPs were washed and air-dried.

The decrease of TEOS in the reaction medium by six times increases the amount of PS in the final NPs by 6.3 times. Thus, the concentration of TEOS was kept as 50 mM for the next studies.

Then, we determined how the amount of encapsulated PS depends on the amount of PS in the reaction mixture (keeping the amounts of TEOS and base constant). For this, **PS 1** was dissolved in EtOH and then NH_4OH (2.4 mmol, 0.32 M) was added. The mixture was sonicated for 5 min and TEOS (0.375 mmol, 50 mM) dissolved in EtOH was added (Table 3). After 24 h, the NPs were washed and air-dried.

A high concentration of PS in the reaction mixture resulted in more effective encapsulation of the PS into the NPs (Table 3). Moreover, the size of the NPs is changing with the same tendency. This is probably because when the amount of PS was increased in the reaction medium, silica forms bigger pores and the NPs become bigger.

Table 1 Detailed experimental data showing how the amount of encapsulated **PS 1** depends on the amount of base. Each result represents the mean of at least two independent experiments and has a standard deviation lower than 5%

NP	NH_4OH [M]	Total amount of final NPs [mg]	% of PS in final NPs [%]	Size of NPs [nm]
NP 1	0.16	—	—	—
NP 2	0.32	20.0	7.95	58.4 ± 6.5
NP 3	0.64	24.0	5.67	266.6 ± 24.4

Table 2 Detailed experimental data showing how the amount of encapsulated PS depends on the amount of TEOS. Each result represents the mean of at least two independent experiments, and has a standard deviation lower than 5%

NP	TEOS [mM]	Total amount of final NPs [mg]	% of PS in final NPs [%]	Size of NPs [nm]
NP 2	50	20	7.95	58.4 ± 6.5
NP 4	300	134.6	1.27	57.5 ± 10.7

Table 3 Detailed experimental data showing how the amount of encapsulated PS depends on the amount of starting PS. Each result represents the mean of at least two independent experiments, and has a standard deviation lower than 5%

NP	PS [mM]	Total amount of final NPs [mg]	% of PS in final NPs [%]	Size of NPs [nm]
NP 5	0.2	19.7	3.41	48.1 ± 4.6
NP 2	0.4	20	7.95	58.4 ± 6.5
NP 6	1.6	25.5	26.27	104.1 ± 6.2
NP 7	4.0	23.0	48.7	197.3 ± 29.0

Optimized PS–SNP formulation protocol

The most successful results were obtained with the preparation of **NP 7** and, consequently, NPs encapsulating compound **PS 2** (**NP 8**, Table 4) were prepared according to the same procedure. In both cases, the amount of encapsulated PS was almost the same. The same protocol was used to synthesize silica nanoparticles in the absence of a PS (**SNP**) for further comparison and characterization (for details, please see the ESI†).

Table 4 Detailed experimental data showing the differences between encapsulation of **PS 1** (**NP 7**) and **PS 2** (**NP 8**). Each result represents the mean of at least two independent experiments, and has a standard deviation lower than 5%

NP	PS 1 [mM]	PS 2 [mM]	Total amount of final NPs [mg]	% of PS in final NPs [%]	Size of NPs [nm]
NP 7	4.0	–	23.0	48.7	197.3 ± 29.0
NP 8	–	4.0	28.2	36.0	128.3 ± 22.2

SNP and PS–NP characterization

The selected NPs were morphologically and chemically characterized by imaging and spectroscopic techniques. For details, please see the ESI.†

The average size of all NPs was measured by transmission electron microscopy (TEM, Fig S5–S7, ESI†). For the final materials, **NP 7** and **NP 8**, dynamic light scattering (DLS) was also used to determine the size distribution (Fig. S8 and S9, ESI†). The particle size distribution was measured by TEM after drying the sample, and in water dispersion by DLS. The difference in the particle sizes measured by TEM (**NP 7**, 197.3 ± 29.0 nm; **NP 8**, 128.3 ± 22.2 nm) and DLS (**NP 7**, 233.5 nm; **NP 8**, 133.2 nm) showed the common difference between the mean hydrodynamic diameter (measured by DLS) and the size (measured by TEM). Typically the hydrodynamic diameter obtained by DLS is larger than the size gathered by TEM. These NPs have a uniform size distribution and are regular in terms of size and shape. As previously mentioned, particles with a size ranging from 10 to 500 nm accumulate inside tumor cells and therefore the developed NPs have an appropriate size for passive targeting to tumor tissues.

The UV-vis absorption spectra of **NP 7** and **NP 8** were collected after dispersing, respectively, 0.535 and 0.510 mg nanoformulations in 3 mL of distilled water (Fig. S12, ESI†). The nanoformulations show the typical spectra of a free base Por, with the Soret band at 403 nm (**NP 7**) and 407 nm (**NP 8**).

The EDS spectra show the chemical composition of **NP 7** and **NP 8**, where a small percentage of sulphur must be related to the thio-carbohydrate moieties of the Pors (Fig. S10 and S11, ESI†). **PS 1**, **PS 2**, **SNP** and the corresponding **NP 7** and **NP 8** were also analysed by FT-IR (Fig. S13, ESI†). The spectra of both NP formulations show some features of the porphyrins (**PS 1** and **PS 2**) and the sole silica nanoparticles (**SNP**).

The amount of encapsulated PS inside the NPs was calculated by UV-vis spectrophotometry. The final NPs were washed with EtOH until no typical Soret and Q bands were observed in the rinse solvent. The final concentration of PS in the NPs [%] was calculated by subtracting the non-encapsulated PS, determined by absorption measurements, in the rinse solvent.[46] **NP 7** (0.289 μmol mg^{-1}) has a slightly higher concentration of PS per mg of final material than **NP 8** (0.215 μmol mg^{-1}).

Singlet oxygen generation study

Singlet oxygen ($^1O_2$) was determined by an indirect chemical method using 1,3-diphenylisobenzofuran (DPBF) as a $^1O_2$ quencher (for details, please refer to the ESI†). $^1O_2$ was determined for both nanoformulations (**NP 7** and **NP 8**) and their corresponding PSs (**PS 1** and **PS 2**) (Fig. 1) in at least three independent experiments. The free **PS 1** and **PS 2** were tested at concentrations of 0.5 μM. NPs composed of **PS 1** and **PS 2** were tested at concentrations of PS: 12.6 μM (**NP 7**) and 1.6 μM (**NP 8**). Both free PSs oxidized DPBF in a similar manner. In spite of the different amount of PS inside the NPs and the different size of these nanoformulations, the DPBF kinetic decay was similar in the two nanoformulations. From this

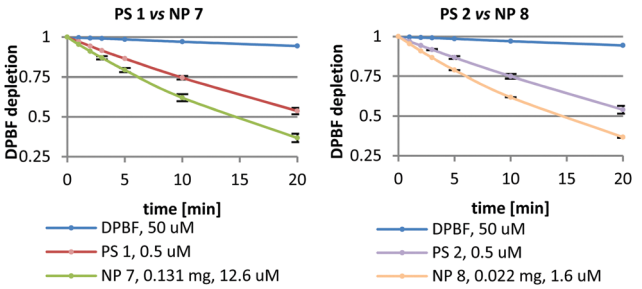

Fig. 1 $^1O_2$ generation by **PS 1**, **PS 2** and their corresponding NPs (**NP 7** and **NP 8**) where each point represents the mean of at least three independent experiments, and has a standard deviation lower than 3%.

study, we can observe that 0.131 mg of **NP 7** could produce the same amount of $^1O_2$ as 0.022 mg of **NP 8**, suggesting that **NP 8** is 6 times more efficient in terms of $^1O_2$ generation. Although **NP 8** (128.3 ± 22.2 nm) is smaller than **NP 7** (197.3 ± 29.0 nm) and has a slightly lower amount of PS per mg of NPs (Table 4), these NPs produce a higher amount of $^1O_2$. This could be due to the fact that in the case of smaller NPs oxygen can penetrate better their pores and $^1O_2$ has a shorter way to go out from the nanoformulation than in bigger NPs. Thus, **NP 8** is more effective in $^1O_2$ production than **NP 7** while the corresponding free Pors (**PS 1** and **PS 2**) produce the same amount of $^1O_2$ under equal experimental conditions.

In vitro studies

In vitro studies were carried out on two human bladder cancer cell lines, HT-1376 and UM-UC-3. These cell lines are suitable as *in vitro* models for the testing of new glyco-porphyrinoids, since the glyco-binding proteins – glucose transporter (GLUT1) and galactose-binding protein (galectin-1) – are abundant but differentially expressed between these two cell lines.[47] Previous studies have demonstrated that these two proteins have a key role in the uptake and further phototoxicity of galactodendritic PSs.[47–51]

Cellular uptake of the PSs and their nanoformulations

Preliminary uptake studies were performed for glucosylated **PS 1** and galactosylated **PS 2** (Fig. 2). Bladder cancer cells were incubated with increasing concentrations of PS (0, 2.5, 5 and 10 μM prepared in PBS, maximum 0.5% DMSO v/v) for 4 h in darkness. Fluorescence spectroscopy studies demonstrated that **PS 1** accumulation was higher in HT-1376 than in UM-UC-3 cancer cells. On the other hand, the uptake of **PS 2** was higher in UM-UC-3 than in HT-1376 cancer cells.

Next, the uptake of **NP 7** and **NP 8** was evaluated by fluorescence spectroscopy and fluorescence microscopy (Fig. 3 and 4) after incubating UM-UC-3 and HT-1376 bladder cancer cells in the dark with different concentrations of the new NPs.

Uptake experiments of both **NP 7** and **NP 8** (for concentrations ranging from 0 to 0.010 mg mL^{-1}) demonstrated that intracellular accumulation was negligible when the cells were incubated with the NPs for 4 h (data not shown). Further studies were performed

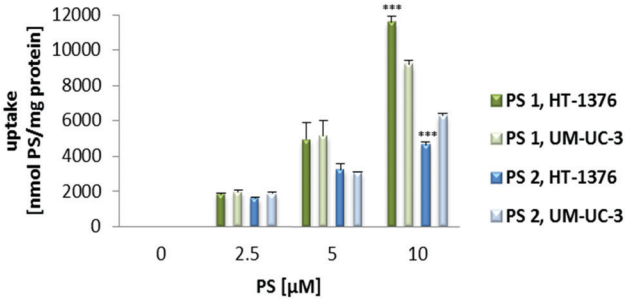

Fig. 2 Cellular uptake of **PS 1** and **PS 2** (0–10 μM in PBS) by UM-UC-3 and HT-1376 bladder cancer cells. Cells were incubated with the PS for 4 h and the uptake was determined by fluorescence spectroscopy. Data are means ± s.e.m. of at least three independent experiments performed in triplicate. ***$P < 0.001$ compared to the PS uptake by UM-UC-3 cancer cells, using Student's *t* test.

by incubating cancer cells with the PS nanoformulations overnight. When the cells were incubated overnight with RPMI medium containing NP solutions, the intracellular accumulation was dependent on the concentration of the NPs and cell line. Interestingly, the uptake of **PS 1** and **PS 2** performed with overnight incubation (PS solutions prepared in cell culture medium) was lower (data not shown) when compared with the uptake of 4 h (PS solutions prepared in PBS buffer). Since we had different incubation conditions, a limitation of this study was that the medium was not present for incubation of the PSs for 4 h. Because of this limitation, the PS uptake may not be comparable for 4 h and 24 h. In addition, the presence of the medium may induce some aggregation effect, both when cells are incubated with the free PSs and after their release from nanoparticles. The uptake of **NP 7** was higher in HT-1376 cells (which contain high levels of GLUT1 protein) when compared with UM-UC-3 cancer cells (Fig. 3). On the other hand, the **NP 8** uptake was higher in UM-UC-3 cells (which contain high levels of galectin-1 protein) than in HT-1376 cancer cells. Considering the levels of galectin-1 and GLUT1 proteins, the uptake of **NP 7** is higher in HT-1376 cells because these NPs contain Por bearing glucose moieties. On the contrary, the higher uptake of **NP 8** in UM-UC-3 cancer cells was

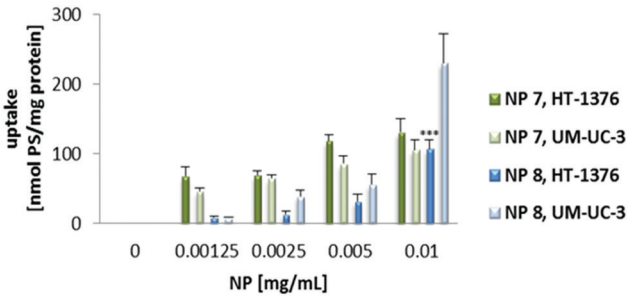

Fig. 3 Cellular uptake of **NP 7** and **NP 8**. UM-UC-3 and HT-1376 bladder cancer cells were incubated with **NP 7** (0–0.010 mg mL^{-1}, 0–2.89 μM of **PS 1** in RPMI medium) and **NP 8** (0–0.010 mg mL^{-1}, 0–2.15 μM of **PS 2** in RPMI medium) overnight. Data are means ± s.e.m. of at least three independent experiments performed in triplicate. ***$P < 0.001$ compared to the NP uptake by UM-UC-3 cancer cells, using Student's *t* test.

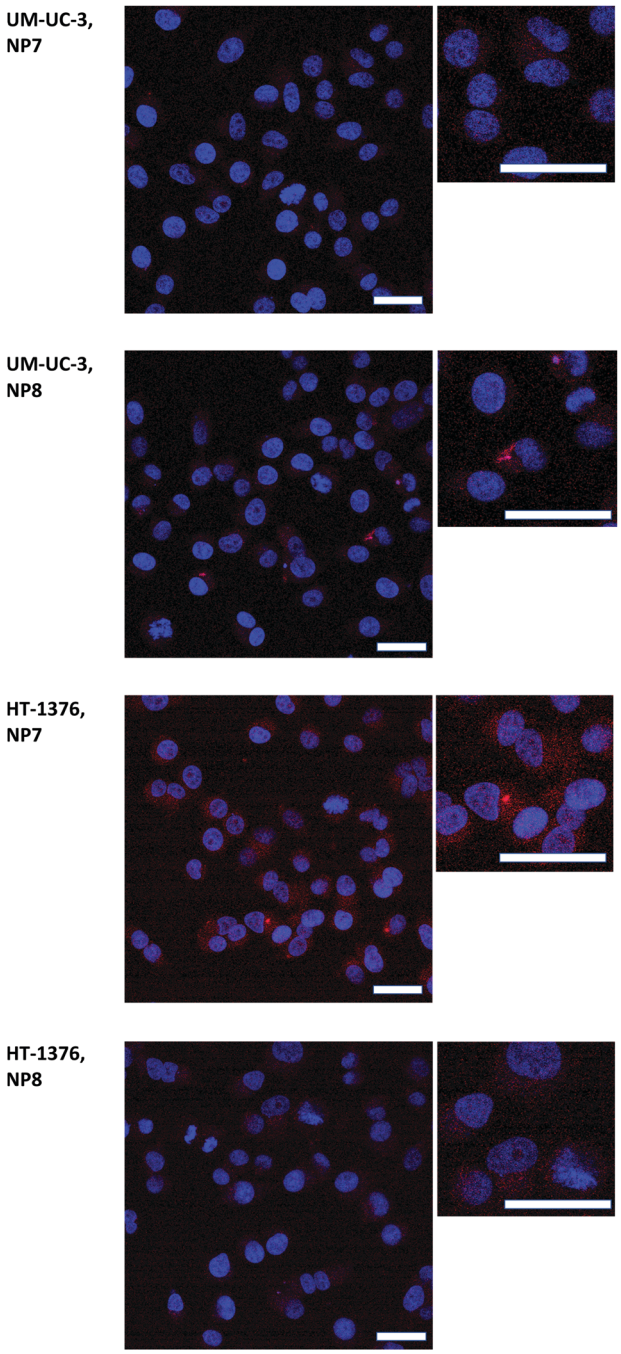

Fig. 4 Representative fluorescence images of UM-UC-3 and HT-1376 bladder cancer cells after overnight incubation with **NP 7** (red, 0.010 mg mL^{-1}, 2.89 μM of **PS 1**) or **NP 8** (red, 0.010 mg mL^{-1}, 2.15 μM of **PS 2**) in darkness and the cell nucleus stained with DAPI (blue). Scale bars, 20 μm.

observed because of Por bearing galactose moieties in the pores of these nanoformulations.

Further studies performed by fluorescence microscopy (Fig. 4) showed preferential intracellular accumulation of **NP 7** and **NP 8** in HT-1376 and UM-UC-3 bladder cancer cells, respectively, when the cells were incubated overnight with 0.010 mg mL^{-1} of the NP formulations (2.89 μM of **PS 1** in the case of **NP 7** and 2.15 μM of **PS 2** for **NP 8**).

Dark toxicity and phototoxicity

The toxicity of **PS 1**, **PS 2**, **NP 7** and **NP 8** in UM-UC-3 and HT-1376 bladder cancer cells in the dark was evaluated using the well-known MTT assay (Fig. S15 and S16, ESI†). This colorimetric assay determines the cell metabolic activity, by assessing the ability of living bladder cancer cells to reduce yellow 3-[4,5-dimethylthiazol-2-yl]-2,5-diphenyl-tetrazolium bromide (MTT) to purple formazan. After overnight incubation of cancer cells (in the dark) with the NPs (0–0.010 mg mL^{-1} in RPMI medium) or 4 h incubation with the PSs (0–10 μM in PBS), none of the PSs or new NPs induced dark toxicity in the cancer cells (Fig. S15 and S16, ESI†). Moreover, during the $^1O_2$ generation studies we observed that the NPs are very much stable in the solution of DMF : H_2O (9 : 1, by volume) in which all experiments were performed (Fig. S3 and S5, ESI†). However, during the biological experiments, slow release of the PS from the silica matrix was detected after 4 h and 18 h incubation in PBS buffer or RPMI medium (Fig. S14, ESI†). Higher release in the case of **NP 8** than in **NP 7** was noted. It could be explained by the fact that **NP 7** (197.3 ± 29.0 nm) is bigger than **NP 8** (128.3 ± 22.2 nm) and thus the PS is more concentrated in **NP 8**. As a result the photosensitizer could be released more easily from **NP 8**.

After confirming the uptake and non-dark toxicity of the PSs and their new NP formulations in UM-UC-3 and HT-1376 bladder cancer cells, their toxicity after light irradiation was equally evaluated using the MTT assay (Fig. 5 and 6). UM-UC-3 and HT-1376 bladder cancer cells were incubated for 4 h with the PSs (0–10 μM in PBS) or overnight with the NPs (**NP 7**: 0–0.010 mg mL^{-1}, 0–2.89 μM of **PS 1** and **NP 8**: 0–0.010 mg mL^{-1}, 0–2.15 μM of **PS 2**) and then irradiated with an optical fiber emitting white light for 40 min (12 mW cm^{-2}). No cytotoxicity was observed in the untreated (cells incubated in the absence of PSs or NPs) sham irradiated cells.

Both the PSs and NPs induced phototoxicity in UM-UC-3 and HT-1376 bladder cancer cells in a concentration- and cell line-dependent manner. However, in the case of the NPs the phototoxicity is much more dependent on the cell line type than on the PSs (Fig. 5 and 6). **NP 7** led to significantly higher phototoxicity on HT-1376 cells compared to UM-UC-3 cells (Fig. 6). The phototoxicity of **NP 8** was higher in UM-UC-3 than in HT-1376 bladder cancer cells (Fig. 8). Taking into account the levels of galectin-1 and GLUT1 proteins, the phototoxicity of **NP 7** is higher in HT-1376 cells compared to UM-UC-3 cells because the uptake of these NPs was higher due to the presence of Por bearing glucose moieties. All the same, the higher phototoxicity of **NP 8** in UM-UC-3 cancer cells was due to the higher uptake by these cells because of Por bearing galactose moieties. The different size of the two nanoformulations could also have some influence on these data; however, under PDT it is expected that the main biological behavior arises from the PS concentration and less from the nanoparticle size. SNPs without PSs did not induce phototoxicity in UM-UC-3 and HT-1376 bladder cancer cells (data not shown).

Taking into account the concentration of PSs inside the NPs, the phototoxicity was shown to be higher with the NP formulations than with the free PSs (Fig. 5–7). From the below figure it is clear that these new nanomaterials are more efficient in PDT than the corresponding free Pors (Fig. 7). **NP 7** with 2.89 μM of **PS 1** was able to induce a pronounced decrease in the HT-1376

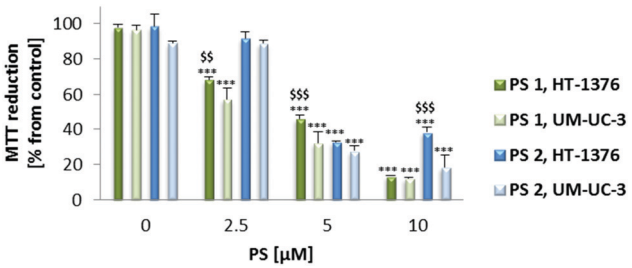

Fig. 5 Phototoxicity of **PS 1** and **PS 2** (0–10 μM in PBS) determined 24 h after PDT treatment using the MTT assay. The percentage of cytotoxicity was calculated relative to control cells (cells incubated with PBS and then irradiated). Data are means ± s.e.m. of at least three independent experiments performed in triplicate. $^{**}P < 0.01$, $^{***}P < 0.001$ compared to MTT reduction in control cells, using Student's *t* test. $^{\$\$}P < 0.01$, $^{\$\$\$}P < 0.001$ compared to MTT reduction by UM-UC-3 cancer cells, using Student's *t* test.

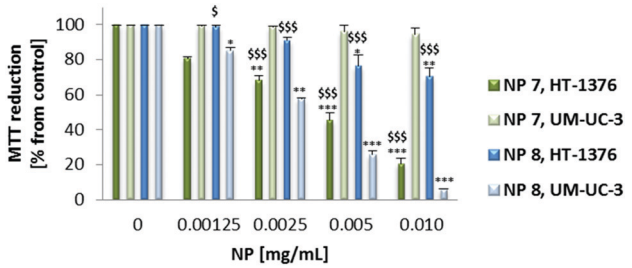

Fig. 6 Phototoxicity of **NP 7** (0–0.010 mg mL^{-1}, 0–2.89 μM of **PS 1**) and **NP 8** (0–0.010 mg mL^{-1}, 0–2.15 μM of **PS 2**) determined 24 h after PDT treatment using the MTT assay. The percentage of cytotoxicity was calculated relative to control cells (cells incubated with RPMI medium and then irradiated). Data are means ± s.e.m. of at least three independent experiments performed in triplicate. $^{*}P < 0.05$, $^{**}P < 0.01$, $^{***}P < 0.001$ compared to MTT reduction in control cells, using Student's *t* test. $^{\$\$}P < 0.01$, $^{\$\$\$}P < 0.001$ compared to MTT reduction by UM-UC-3 cancer cells, using Student's *t* test.

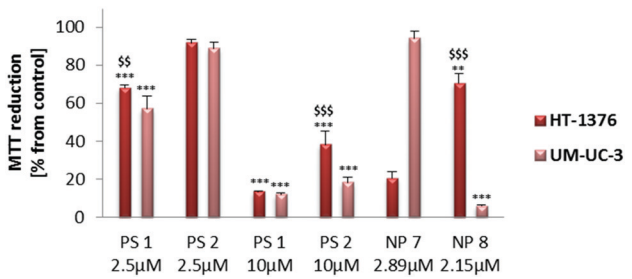

Fig. 7 Phototoxicity of **PS 1** (2.5 μM, 10 μM), **PS 2** (2.5 μM, 10 μM), **NP 7** (2.89 μM of **PS 1**) and **NP 8** (2.15 μM of **PS 2**) determined 24 h after PDT treatment using the MTT assay. The percentage of cytotoxicity was calculated relative to control cells (cells incubated with RPMI medium and then irradiated). Data are means ± s.e.m. of at least three independent experiments performed in triplicate. $^{**}P < 0.01$, $^{***}P < 0.001$ compared to MTT reduction in control cells, using Student's *t* test. $^{\$\$}P < 0.01$, $^{\$\$\$}P < 0.001$ compared to MTT reduction by UM-UC-3 cancer cells, using Student's *t* test.

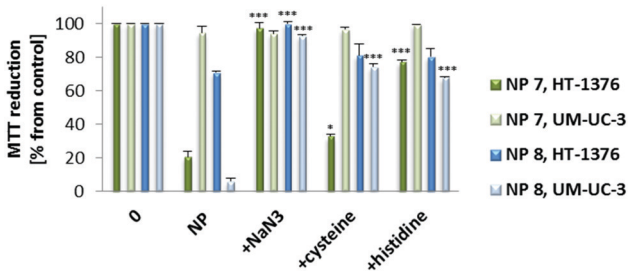

Fig. 8 Phototoxicity after PDT with **NP 7** (0.010 mg mL^{-1}, 2.89 μM of **PS 1**) and **NP 8** (0.010 mg mL^{-1}, 2.15 μM of **PS 2**) in the presence of 50 nM of ROS quenchers (sodium azide, histidine and cysteine) in HT-1376 and UM-UC-3 cells. Cytotoxicity was assessed 24 h after treatment using the MTT assay. The percentage of cytotoxicity was calculated relative to control cells (untreated cells). Data are means ± s.e.m. of at least three independent experiments performed in triplicate. *$P < 0.05$, ***$P < 0.001$ compared to MTT reduction (%) 24 h after PDT with NPs using Student's *t* test.

cell viability, which was similar to 10 μM of free **PS 1**. Likewise, **NP 8** with 2.15 μM of **PS 2** was able to induce a similar decrease in the UM-UC-3 cell viability to 10 μM of free **PS 2**. Thus, these NPs are around 3–5 times more effective in photodynamic therapy activity than the respective free Pors.

The role of cytotoxic ROS generated after PDT with 0.010 mg mL^{-1} of **NP 7** (2.89 μM of **PS 1**) and **NP 8** (2.15 μM of **PS 2**) was evaluated using sodium azide, histidine[52] and cysteine[53] as ROS quenchers (Fig. 8). When PDT experiments were performed with cells in the presence of non-toxic concentrations of ROS quenchers, there was a reduction in the phototoxicity induced by the new NPs. The data show that $^1O_2$ should have a high effect on the phototoxicity induced by **NP 7** or **NP 8**, since the phototoxicity was highly reduced when PDT experiments were performed with $^1O_2$ quenchers (sodium azide and histidine).

Conclusions

In summary, two types of new glyco-PS loaded SNPs were successfully prepared after modification and optimization of the well-known Stöber method. Both novel materials were able to produce $^1O_2$ and hence *in vitro* studies with two human bladder cancer cell lines, HT-1376 and UM-UC-3, were performed. Despite slightly lower efficiency in terms of singlet oxygen generation compared to non-immobilized PSs, the nanocarriers offer an alternative route to develop new platforms for PDT. Overall, these NPs demonstrated 3–5 times higher therapeutic efficacy *in vitro* compared with the corresponding free PSs. In the presented work, we demonstrated that *S*-glycoside Pors encapsulated into a silica matrix by a straightforward Stöber method were more efficient in *in vitro* PDT against two human bladder cancer cell lines, HT-1376 and UM-UC-3, than non-encapsulated PSs.

Conflicts of interest

There are no conflicts to declare.

Acknowledgements

Thanks are due to FCT/MEC for the financial support to QOPNA (FCT UID/QUI/00062/2019), CICECO-Aveiro Institute of Materials (UIDB/50011/2020), CIBB (UIDB/04539/2020) and CQE (UIDB/00100/2020) research units, through national funds and where applicable cofinanced by the FEDER, within the PT2020 Partnership Agreement. The authors also acknowledge FCT for the doctoral research fellowship SFRH/BD/85941/2012 (to PMRP). The work was also supported by the Spanish MINECO (CTQ2017-85393-P) and ERA-NET/MINECO (EuroNanoMed2017-191/PCIN-2017-042) and Portuguese COMPETE (POCI-01-0145-FEDER-007440). We further wish to thank the Seventh Framework Programme (FP7-People-2012-ITN) for funding the SO2S project (grant agreement number: 316975).

Notes and references

1 R. Bonnett, *Chem. Soc. Rev.*, 1995, **24**, 19–33.
2 P.-C. Lo, M. S. Rodríguez-Morgade, R. K. Pandey, D. K. P. Ng, T. Torres and F. Dumoulin, *Chem. Soc. Rev.*, 2020, **49**, 1041–1056.
3 D. E. J. G. J. Dolmans, D. Fukumura and R. K. Jain, *Nat. Rev. Cancer*, 2003, **3**, 380–387.
4 I. J. Macdonald and T. J. Dougherty, *J. Porphyrins Phthalocyanines*, 2001, **05**, 105–129.
5 C. Liang, X. Zhang, Z. Wang, W. Wang, M. Yang and X. Dong, *J. Mater. Chem. B*, 2020, **8**, 4748–4763.
6 H. Abrahamse and M. R. Hamblin, *Biochem. J.*, 2016, **473**, 347–364.
7 D. K. Chatterjee, L. S. Fong and Y. Zhang, *Adv. Drug Delivery Rev.*, 2008, **60**, 1627–1637.
8 N. M. Idris, M. K. Gnanasammandhan, J. Zhang, P. C. Ho, R. Mahendran and Y. Zhang, *Nat. Med.*, 2012, **18**, 1580–1586.
9 H. S. Qian, H. C. Guo, P. C.-L. Ho, R. Mahendran and Y. Zhang, *Small*, 2009, **5**, 2285–2290.
10 Y. Zhou, X. Liang and Z. Dai, *Nanoscale*, 2016, **8**, 12394–12405.
11 V. Almeida-Marrero, E. van de Winckel, E. Anaya-Plaza, T. Torres and A. de la Escosura, *Chem. Soc. Rev.*, 2018, **47**, 7369–7400.
12 P. Couleaud, V. Morosini, C. Frochot, S. Richeter, L. Raehma and J.-O. Durand, *Nanoscale*, 2010, **2**, 1083–1095.
13 H. Kobayashi, R. Watanabe and P. L. Choyke, *Theranostics*, 2014, **4**, 81–89.
14 H. Maeda, *Bioconjugate Chem.*, 2010, **21**, 797–802.
15 L. Tang and J. Cheng, *Nano Today*, 2013, **8**, 290–312.
16 S. Heidegger, Go, A. Schmidt, S. Niedermayer, C. Argyo, S. Endres, T. Bein and C. Bourquin, *Nanoscale*, 2016, **8**, 938–948.
17 W. Q. Lim, S. Z. F. Phua, H. V. Xu, S. Sreejith and Y. Zhao, *Nanoscale*, 2016, **8**, 12510–12519.
18 X. Yao, X. Chen, C. He, L. Chen and X. Chen, *J. Mater. Chem. B*, 2015, **3**, 4707–4714.
19 J. G. Croissant, S. Picard, D. Aggad, M. Klausen, C. Mauriello Jimenez, M. Maynadier, O. Mongin, G. Clermont, E. Genin,

X. Cattoën, M. Wong Chi Man, L. Raehm, M. Garcia, M. Gary-Bobo, M. Blanchard-Desce and J.-O. Durand, *J. Mater. Chem. B*, 2016, **4**, 5567–5574.
20 V. Biju, *Chem. Soc. Rev.*, 2014, **43**, 744–764.
21 C. R. Steven, G. A. Busby, C. Mather, B. Tariq, M. L. Briuglia, D. A. Lamprou, A. J. Urquhart, M. H. Grant and S. V. Patwardhan, *J. Mater. Chem. B*, 2014, **2**, 5028–5042.
22 C. M. Dawidczyk, C. Kim, J. H. Park, L. M. Russell, K. H. Lee, M. G. Pomper and P. C. Searson, *J. Controlled Release*, 2014, **187**, 133–144.
23 G. Pillai, *SOJ Pharm. Pharm. Sci*, 2014, **1**, 1–13.
24 G. Pillai and M. L. Ceballos-Coronel, *SAGE Open Med.*, 2013, **1**, 1.
25 G. Obaid, M. Broekgaarden, A.-L. Bulin, H.-C. Huang, J. Kuriakose, J. Liu and T. Hasan, *Nanoscale*, 2016, **8**, 12471–12503.
26 D. Lombardo, M. A. Kiselev and M. T. Caccamo, *J. Nanomater.*, 2019, **2019**, 26.
27 L. Shang, K. Nienhaus and G. U. Nienhaus, *J. Nanobiotechnol.*, 2014, **12**, 5.
28 V. Torchilin, *Adv. Drug Delivery Rev.*, 2011, **63**, 131–135.
29 S. Biswas and V. P. Torchilin, *Adv. Drug Delivery Rev.*, 2014, **66**, 26–41.
30 F. Figueira, J. A. S. Cavaleiro and J. P. C. Tomé, *J. Porphyrins Phthalocyanines*, 2011, **15**, 517–533.
31 W. Borzęcka, T. Trindade, T. Torres and J. Tomé, *Curr. Pharm. Des.*, 2016, **22**, 6021–6038.
32 R. K. Fei Yan, *Photochem. Photobiol.*, 2003, **78**, 587–591.
33 W. Li, W. Lu, Z. Fan, X. Zhu, A. Reed, B. Newton, Y. Zhang, S. Courtney, P. T. Tiyyagura, S. Li, E. Butler, H. Yu, P. C. Ray and R. Gao, *J. Mater. Chem.*, 2012, **22**, 12701–12708.
34 J. Qian, D. Wang, F. Cai, Q. Zhan, Y. Wang and S. He, *Biomaterials*, 2012, **33**, 4851–4860.
35 I. T. Teng, Y.-J. Chang, L.-S. Wang, H.-Y. Lu, L.-C. Wu, C.-M. Yang, C.-C. Chiu, C.-H. Yang, S.-L. Hsu and J.-a. A. Ho, *Biomaterials*, 2013, **34**, 7462–7470.
36 X. Deng, L. Xiong, L. Lin, G. Xiong and X. Miao, *Photodiagn. Photodyn. Ther.*, 2013, **10**, 460–469.
37 Z.-T. Liu, L. Xiong, Z.-P. Liu, X.-Y. Miao, L.-W. Lin and Y. Wen, *Nanoscale Res. Lett.*, 2014, **9**, 319–327.
38 L. Dongyu, Z. Hequn, C. Liliang, Z. Xinyuan and Q. Jun, *Opt. Quantum Electron.*, 2015, **47**, 3081–3090.
39 X. Chen, L. Hui, D. A. Foster and C. M. Drain, *Biochemistry*, 2004, **43**, 10918–10929.
40 S. Shiho HirohHirohara, M. Obata, H. Alitomo, K. Sharyo, T. Ando, S. Yano and M. Tanihara, *Bioconjugate Chem.*, 2009, **20**, 944–952.
41 S. Singh, A. Aggarwal, S. Thompson, J. P. C. Tomé, X. Zhu, D. Samaroo, M. Vinodu, R. Gao and C. M. Drain, *Bioconjugate Chem.*, 2010, **21**, 2136–2146.
42 S. Hirohara, M. Nishida, K. Sharyo, M. Obata, T. Ando and M. Tanihara, *Bioorg. Med. Chem.*, 2010, **18**, 1526–1535.
43 S. Hirohara, M. Obata, H. Alitomo, K. Sharyo, T. Ando, M. Tanihara and S. Yano, *J. Photochem. Photobiol., B*, 2009, **97**, 22–33.
44 X. Chen, L. Hui, D. A. Foster and C. M. Drain, *Biochemistry*, 2004, **43**, 10918–10929.
45 W. Stober and A. Fink, *J. Colloid Interface Sci.*, 1968, **26**, 62–69.
46 C. M. B. Carvalho, E. Alves, L. Costa, J. P. C. Tomé, M. A. F. Faustino, M. G. P. M. S. Neves, A. C. Tomé, J. A. S. Cavaleiro, A. Almeida, Â. Cunha, Z. Lin and J. Rocha, *ACS Nano*, 2010, **4**, 7133–7140.
47 P. M. R. Pereira, S. Silva, J. A. S. Cavaleiro, C. A. F. Ribeiro, J. P. C. Tomé and R. Fernandes, *PLoS One*, 2014, **9**, e95529.
48 S. Silva, P. M. R. Pereira, P. Silva, F. A. A. Paz, M. A. F. Faustino, J. A. S. Cavaleiro and J. P. C. Tome, *Chem. Commun.*, 2012, **48**, 3608–3610.
49 P. M. R. Pereira, S. Silva, J. S. Ramalho, C. M. Gomes, H. Girão, J. A. S. Cavaleiro, C. A. F. Ribeiro, J. P. C. Tomé and R. Fernandes, *Eur. J. Cancer*, 2016, **68**, 60–69.
50 P. M. R. Pereira, S. Silva, M. Bispo, M. Zuzarte, C. Gomes, H. Girão, J. A. S. Cavaleiro, C. A. F. Ribeiro, J. P. C. Tomé and R. Fernandes, *Bioconjugate Chem.*, 2016, **27**, 2762–2769.
51 P. M. R. Pereira, W. Rizvi, N. V. S. D. K. Bhupathiraju, N. Berisha, R. Fernandes, J. P. C. Tomé and C. M. Drain, *Bioconjugate Chem.*, 2018, **29**, 306–315.
52 M. Bancirova, *Luminescence*, 2011, **26**, 685–688.
53 O. I. Aruoma, B. Halliwell, B. M. Hoey and J. Butler, *Free Radical Biol. Med.*, 1989, **6**, 593–597.